



Synthesis and characterization of nanostructured carbon-supported Pt electrocatalysts for membraneless methanol fuel cells (MLMFC)

S.P.R. Kalaikathir¹ and S. Begila David^{2*}

¹Department of Chemistry, Womens' Christian College, Nagercoil – 629 001, India.

²PG and Research Centre in Chemistry, Scott Christian College (Autonomous), Nagercoil – 629 003, India.

Abstract : Carbon-supported Pt–Ru–Fe/C (70:20:10), Pt–Ru–Fe/C (70:15:15), Pt–Ru–Fe/C (70:10:20), Pt–Ru/C (50:50), Pt–Fe/C (50:50) and Pt/C (100) electrocatalysts were synthesized by co-impregnation reduction method. The physicochemical characterizations demonstrated that all the compositions have the Pt face-centered cubic (fcc) structure with variations in the lattice parameter, indicating the incorporation of Ru and Fe. Transmission electron microscopy measurements revealed a decrease in the mean particle size of the catalysts for the ternary compositions. The electrochemical characterization showed that binary and ternary electrocatalysts have higher catalytic activity than Pt/C toward methanol electrooxidation. Voltammetric data showed the addition of Fe to Pt–Ru/C significantly diminished the potential of methanol and CO oxidation, due to the electronic effect exerted by this metal along with the bifunctional mechanism. Single cell tests on a membraneless methanol fuel cell at room temperature with Pt–Ru–Fe/C (70:20:10) showed superior performance compared to Pt–Ru–Fe/C (70:15:15), Pt–Ru–Fe/C (70:10:20), Pt–Ru/C (50:50), Pt–Fe/C (50:50) and Pt/C (100) electrocatalysts. The i-V characteristic curve indicated an enhancement in fuel cell performance with the addition of Fe and Ru to Pt-catalyst.

Keywords: Co-impregnation reduction, Membraneless fuel cells, Methanol, Platinum, Ruthenium, Iron, Sodium perborate.

Introduction

Fuel cells are eco-friendly power source that convert hydrogen and oxygen into electrical energy along with the production of heat and water by oxidoreduction reactions. Several different types of fuel cells are currently under development, with a variety of targeted applications ranging from miniature power supplies to large-scale power plants. Small fuel cells have received much interest in recent years as a potential power source for the generation of portable electronic devices. One class of microstructured power supply is microfluidic fuel cells or laminar flow-based fuel cells and membraneless fuel cells [1]. A microfluidic fuel cell is a device that confines all the fundamental components of a fuel cell into a single microstructured manifold [2]. Microfluidic membraneless fuel cells eliminate the use of proton exchange membrane as they utilize the co-laminar flow nature of multistream in a single microfluidic channel to separate the anolyte and the catholyte [3]. Microfluidic membraneless fuel cells avoid several issues associated with polymer electrolyte membrane-based fuel cells such as humidification, membrane degradation, water management, and fuel crossover. Moreover, miniaturization of membraneless fuel cells has drawn significant interest because of their potential advantages,

including compact design, high-energy conversion efficiency, low operating temperature, environmental-friendly emissions, use of both metallic and biological catalysts, and elimination of the moving parts [4]. Methanol is considered as one of the most promising combustible materials used in fuel cells, because of its high-energy storage ($5,019 \text{ A h Kg}^{-1}$), low toxicity, large-scale production from biomass, easy storage and transportation, and facile electro-oxidation on Pt catalyst. It is renewable, and its complete oxidation to CO_2 and H_2O produces a high yield of 6 electrons per molecule in acid electrolyte as shown in Eq. (1).



However, methanol electro-oxidation on pure platinum encounters many problems such as the difficulties in adsorption and dehydrogenation of the methanol molecule and the formation of CO-intermediates that poison the Pt anode catalysts. The slow kinetics of the methanol electro-oxidation reaction (MOR) on Pt anode diminishes the overall performance of the MLMFC system [5]. Considerable efforts have been directed toward the development of effective electrocatalysts that can oxidize methanol at lower potentials. For example, alloying of Pt with other elements such as Ru, Sn, Mo, W, Pd, Ni, Rh and Ir have been studied, and among them, Ru has shown the best catalytic effect on MOR [6-8]. The second metal of the co-catalysts shows bifunctional mechanism and has a ligand effect [9,10]. Nevertheless, it is still an ongoing task to improve the performance of Pt–Ru anode catalyst to a level suitable for commercialization.

To further improve Pt–Ru/C electrocatalyst's activity, a third metal M is introduced into their composition, which helps to enhance the dehydrogenation reaction and the CO tolerance of the catalysts during the oxidation of methanol [11]. Numerous investigations have reported that the Pt–Ru–M composition displays excellent activity for the oxidation of methanol. Neto *et al.* [12] investigated the electro-oxidation of methanol and ethanol with Pt–Ru–Sn ternary alloy catalysts prepared via an alcohol-reduction process using ethylene glycol as the solvent and a reduction agent. Jeon *et al.* [13] also observed that Pt–Ru–Ni/C electrocatalyst prepared by NaBH_4 reduction was more active for methanol oxidation than a commercial Pt–Ru/C electrocatalyst. Chen *et al.* [14] prepared a Pt–Ru ternary alloy by the sodium borohydride (NaBH_4)-reduction method to compare the study of tungsten-modified Pt–Ru electrocatalysts for methanol oxidation. And, more recently, Scofield *et al.* [15] studied the composition of ultrathin, ternary alloy Pt–Ru–Fe nanowires for the methanol oxidation reaction and formic acid oxidation reaction. They observed that the methanol oxidation appears to be predominantly influenced by the Ru content, whereas formic acid oxidation is primarily impacted by the corresponding Fe content within the ternary metal alloy catalyst itself. The enhanced activity of the ternary catalyst is due to the promoting effect of the second or third elements added to Pt. Moreover, the main advantage of the introduction of the third metal is the reduction of the oxidation potential of small organic molecules, coupled with the rise in current density. In the present study, we evaluated the catalytic activity for the methanol electro-oxidation reaction by incorporating a third metal Fe to the Pt–Ru catalyst on a carbon support in membraneless methanol fuel cell (MLMFC). The performance of the Pt–Ru–Fe/C catalyst was compared with that of the Pt–Ru/C and Pt–Fe/C catalysts obtained by the co-impregnation reduction method.

Experimental

Material

The metal precursors used for the preparation of electrocatalysts were $\text{H}_2\text{PtCl}_6 \cdot 6\text{H}_2\text{O}$ (from Aldrich), $(\text{NH}_4)_2\text{Fe}(\text{SO}_4)_2$ (from Alfa Aesar), and $\text{RuCl}_3 \cdot 3\text{H}_2\text{O}$ (from Merck). Vulcan Carbon XC-72 (from Cabot Corp.) was used as a support for the catalysts. Graphite plates (3 cm long and 0.1 cm wide, from E-TEK) were used as substrates for the catalyst to prepare the electrodes. Iso-propanol and sodium borohydride (from Merck) was used as the solvent and reduction agent respectively. Nafion[®] (DE 521, DuPont USA) dispersion was used to make the catalyst ink. Methanol (from Merck), sodium percarbonate (from Riedel) and H_2SO_4 (from Merck) were used as the fuel, the oxidant and as the electrolyte for electrochemical analysis, respectively. All the chemicals were of analytical grade. Pt/C (40-wt%, from E-TEK) was used as the cathode catalyst.

Preparation of Pt–Ru–Fe/C catalysts

Carbon-supported ternary Pt–Ru–Fe catalysts with different atomic ratios were synthesized by co-impregnation reduction method [12,16]. The precursors were first suspended in iso-propanol and ultrasonicated for 3h. The carbon support Vulcan XC-72R, was preheated to 110°C for 2h and suspended in iso-propanol

separately and ultrasonicated for 3 h. Precursor suspension is then added drop wise to carbon slurry [17]. The weight ratio of Pt–X/C (X = Fe, Ru, Ru–Fe) was controlled according to the targeted metal loading. Ultrasonic blending for 3h, of precursor and carbon suspension was carried out to ensure the proper impregnation of metal precursors on carbon support. The suspension was then kept at 70°C for 12 h to evaporate iso-propanol. To reduce metal precursors 0.2 M NaBH₄ solution was added to the mixture with stirring and further stirred for 3 h to confirm termination of reduction reaction. Finally the precipitate was collected by filtration, washed with deionized (DI) water, and dried at 70°C for 2 h. The electrocatalytic mixtures and the atomic ratios were Pt/C (100), Pt–Ru/C (50:50), Pt–Fe/C (50:50), Pt–Ru–Fe/C (70:10:20), Pt–Ru–Fe/C (70:15:15) and Pt–Ru–Fe/C (70:20:10). The nominal loading of metals in the electrocatalysts was 40% wt. and the remaining was 60% wt. carbon.

Preparation of the working electrode

The catalyst ink was prepared by mixing 50 mg of carbon supported catalyst powder and 1 mL of Nafion solution (5 wt.%) in 5 mL ultrapure water (Millipore MilliQ, 18 MΩ cm). 3 μL of ultrasonically homogenized ink was deposited onto a freshly polished glassy-carbon electrode before each experiments and the solvent was then evaporated in open air at room temperature. The loading of metal on the working electrode was 0.28 mg_{metal}/cm².

Physical characterization of the catalysts

The morphology of the dispersed catalysts was examined using SEM (ZEISS EVO 50 Scanning Electron Microscope) and TEM (Philips CM 12 Transmission Electron Microscope). The particle size distribution and mean particle size were also evaluated using TEM. The crystal structure of the synthesized electrocatalysts was characterized by powder X-ray diffraction (XRD) using a Rigaku multiflex diffractometer (model RU-200 B) with Cu-K_{α1} radiation source ($\lambda_{K\alpha1} = 1.5406 \text{ \AA}$) operating at room temperature. The tube current was 40 mA with a tube voltage of 40 kV. The 2θ angular regions between 20° and 90° were recorded at a scan rate of 5° min⁻¹. The mean particle size analyzed from TEM is verified by determining the crystallite size from XRD pattern using Scherrer formula [18]. Pt (2 2 0) diffraction peak was selected to calculate crystallite size and lattice parameter of platinum. According to Scherrer's equation shown in Eq. (2):

$$d = \frac{0.9\lambda_{K\alpha1}}{\beta_{2\theta} \cos \theta_{\max}} \quad (2)$$

where d is the average crystallite size, θ_{\max} is the angle at the position of the peak maximum, $\beta_{2\theta}$ is the width of the peak (in radians), 0.9 is the shape factor for spherical crystallite and $\lambda_{K\alpha1}$ is the wavelength of X-rays used. The lattice parameters of the catalysts were estimated according to Eq. 3 [19]:

$$a = \frac{\sqrt{2} \lambda_{K\alpha1}}{\sin \theta_{\max}} \quad (3)$$

where a, is the lattice parameter (nm) and all the other symbols have the same meanings as in Eq. 1. The atomic ratio of the catalysts was determined by an energy dispersive X-ray (EDX) analyzer, which was integrated with the TEM instrument.

Electrochemical measurements

The electrochemical experiments were carried out in a conventional three-electrode cell at room temperature. Voltammetric curves using 0.5 M H₂SO₄ or 1 M C₂H₅OH/0.5 M H₂SO₄ electrolyte solutions purged with nitrogen gas were recorded with an electrochemical workstation (CHI-6650; CH Instruments, USA). Catalyst coated glassy-carbon electrode was used as the working electrode and a platinum wire was used as the counter electrode. Ag/AgCl in saturated KCl was used as the reference electrode. The activity of the

electrocatalysts was determined by cyclic voltammetry in a half cell at a scan rate of 50 mVs^{-1} between 0.05 and 1.2 V vs. Ag/AgCl and chronoamperometry (0.4 V vs. Ag/AgCl for 30 minutes).

Single cell test

In the present study, we fabricated the membraneless methanol fuel cell (MLMFC) using laminar flow-based fuel cell configuration [20-23]. In this membraneless fuel cell, methanol is used as a fuel, sodium percarbonate is used as an oxidant and sulphuric acid is used as an electrolyte. Sodium percarbonate ($2\text{Na}_2\text{CO}_3 \cdot 3\text{H}_2\text{O}_2$) is a cheap, environment friendly, nontoxic, and large-scale industrial chemical, primarily used as a source of 'active oxygen' in detergents and as a mild antiseptic. In crystalline state sodium percarbonate exists as a dimeric peroxy-salt with water of hydration, but in aqueous solution affords hydrogen peroxide [24] as shown in Eq. (4).



The byproduct is completely innocuous and this stable and easily handled crystalline substance is used as oxidant in our MLMFC.

In MLMFC, the aqueous fuel and oxidant streams flow in parallel in a single microchannel with the anode and cathode on opposing sidewalls (Fig. 1). Graphite plates of one mm thickness served as current collectors and catalyst support structures. The anode catalysts with different atomic ratios were coated onto the graphite plates. For single cell, the anode catalysts were prepared as follows: The catalyst ink was prepared by mixing 100 μL of Nafion (5 wt.% from DuPont) solution, 1 mL of isopropanol and 15 mg of catalytic powder. This mixture was then brushed on a graphite plate in 3 cm^2 areas and dried at $100 \text{ }^\circ\text{C}$ for 30 min to give an approximate total metal loading of 2 mg/cm^2 on the anode. The catalysts tested on the anode side were Pt/C (100), Pt-Ru/C (50:50), Pt-Fe/C (50:50), Pt-Ru-Fe/C (70:10:20), Pt-Ru-Fe/C (70:15:15) and Pt-Ru-Fe/C (70:20:10). On the cathode side, Pt/C (100) with catalyst loading 2 mg/cm^2 was used in all experiments.

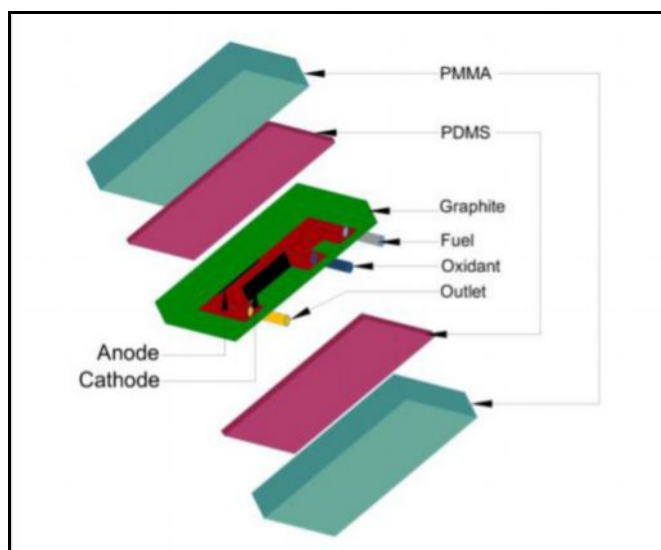


Fig. 1 Schematic of the E-shaped membraneless laminar flow-based fuel cell with catalyst-coated graphite plates molded with poly(dimethylsiloxane) (PDMS) and sealed with poly(methylmethacrylate) (PMMA)

The two catalyst-coated graphite plates were aligned to form a channel with 0.1 cm electrode-to-electrode distance (width), a 3 cm length, and a 0.1 cm height. The anolyte (fuel and electrolyte) and catholyte (oxidant and electrolyte) streams flow in a laminar fashion over the anode and cathode, respectively. The electrode area along a microchannel wall between the inlets and the outlet (3 cm long and 0.1 cm wide) was used as the geometric surface area of the electrodes in this study (0.3 cm^2). The design is described in detail elsewhere [25]. The anolyte used in the anode side was 1.0 M methanol + 0.5 M H_2SO_4 and the catholyte used in the cathode side was 0.1 M percarbonate + 0.5 M H_2SO_4 . The flow rate of each of the streams was 0.3 mL min^{-1} (total flow rate of 0.6 mL min^{-1}). In multistream laminar flow, two or more liquid streams merge into a

single microfluidic channel and continue to flow laminarily in parallel without turbulent mixing. The MLMFC was operated at room temperature. The current-voltage characteristics of MLMFC were measured using an electrochemical workstation (CH Instruments, model CHI6650, USA) and the data was verified using a multi-meter (MASTECH[®] MAS830L).

Results and discussions

Physical characterization

X-ray diffraction (XRD)

The XRD patterns of the prepared Pt–Ru/C (50:50), Pt–Fe/C (50:50), Pt–Ru–Fe/C (70:10:20), Pt–Ru–Fe/C (70:15:15) and Pt–Ru–Fe/C (70:20:10) catalysts are shown in Fig. 2. The diffraction peaks seen in all the diffraction patterns at around 25–30° are associated with (0 0 2) plane of hexagonal structure of Vulcan XC-72 carbon support. The diffractogram of Pt–Ru/C electrocatalyst show peaks at around 40°, 47°, 67° and 82°, which are associated with the (1 1 1), (2 0 0), (2 2 0) and (3 1 1) crystalline planes respectively, of the face centered cubic (fcc) structure characteristic of platinum and platinum alloys. No peaks corresponding to a metallic ruthenium or the ruthenium oxides were detected in the Pt–Ru–Fe catalysts, but their presence cannot be discarded because they may be present in a very small particle size or even in an amorphous form [26]. The Pt–Fe/C electrocatalyst also showed the peaks characteristic of the fcc structure of platinum and platinum alloys similar to Pt–Ru/C electrocatalysts. However, in this sample two additional peaks were observed at 35° that were identified as a γ -Fe₂O₃ phase [18]. The fcc lattice parameters were evaluated from the angular position of the (2 2 0) peaks and the calculated value for Pt–Ru/C electrocatalyst (0.3881 nm) was smaller than that of Pt/C electrocatalyst (0.3912 nm), indicating a contraction of the lattice and a Pt and Ru alloy to some extent. For Pt–Fe/C electrocatalyst the fcc lattice parameter measured (0.3982 nm) was larger than the one obtained for Pt/C electrocatalyst, due to a lattice expansion after alloying, indicating that part of Fe was incorporated in the fcc structure of Pt. The fcc lattice parameters calculated for Pt–Ru–Fe/C electrocatalysts were: Pt–Ru–Fe/C 70:10:20 (0.3932 nm), Pt–Ru–Fe/C 70:15:15 (0.3903 nm) and Pt–Ru–Fe/C 70:20:10 (0.3885 nm). Compared to Pt/C electrocatalyst the fcc lattice parameter was increased in Pt–Ru–Fe/C (70:10:20) electrocatalyst but decreased in Pt–Ru–Fe/C (70:20:10) electrocatalyst. The difference of lattice parameters and the shift of (2 2 0) plane indicate interactions between Pt, Ru, and Fe. The peaks of the γ -Fe₂O₃ phase at 35° were clearly observed for Pt–Ru–Fe/C (70:10:20) and (70:15:15), while for Pt–Ru–Fe/C (70:20:10) only the peaks characteristic of the Pt fcc structure were observed. The average particle size was estimated using the Scherrer equation (Table 1). The particle sizes for Pt–Ru/C, Pt–Fe/C, and Pt–Ru–Fe/C electrocatalysts were in the range of 2.4–4.1 nm.

Table 1 The EDX composition, lattice parameters, and the particle size obtained for different atomic ratios of electrocatalysts

Electrocatalyst	Nominal atomic ratio			EDX Atomic ratio			Lattice parameter (nm)	Crystallite size (nm)	Particle size from TEM (nm)
	Pt	Ru	Fe	Pt	Ru	Fe			
Pt–Fe/C	50	-	50	52	-	48	0.3982	4.1	3.7
Pt–Ru/C	50	50	-	51	49	-	0.3891	3.9	3.6
Pt–Ru–Fe/C	70	10	20	72	9	19	0.3932	3.0	2.5
Pt–Ru–Fe/C	70	15	15	72	16	12	0.3903	2.8	2.2
Pt–Ru–Fe/C	70	20	10	69	18	13	0.3885	2.4	2.0

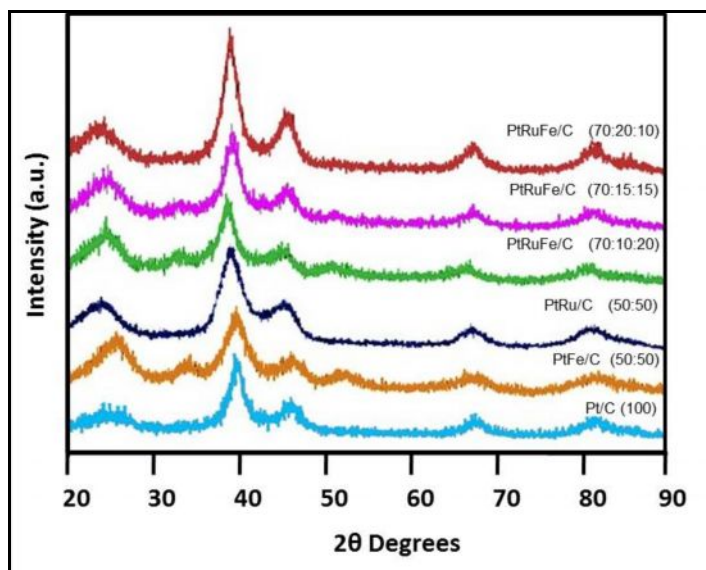


Fig. 2 X-ray diffraction patterns of Pt–Ru–Fe/C (70:20:10), Pt–Ru–Fe/C (70:15:15), Pt–Ru–Fe/C (70:10:20), Pt– Ru/C (50:50), Pt–Fe/C (50:50) and Pt/C (100) catalysts

Scanning electron microscopy (SEM)

SEM images of Pt/C, Pt–Fe/C, Pt–Ru/C and Pt–Ru–Fe/C catalysts prepared are shown in Fig. 3a–d. SEM image clearly shows that the nanoparticles of the catalysts are uniformly dispersed on the carbon support. The particles showing high contrast are of Fe, charged by the electron beam. The SEM images confirm the porous structure of the catalysts prepared.

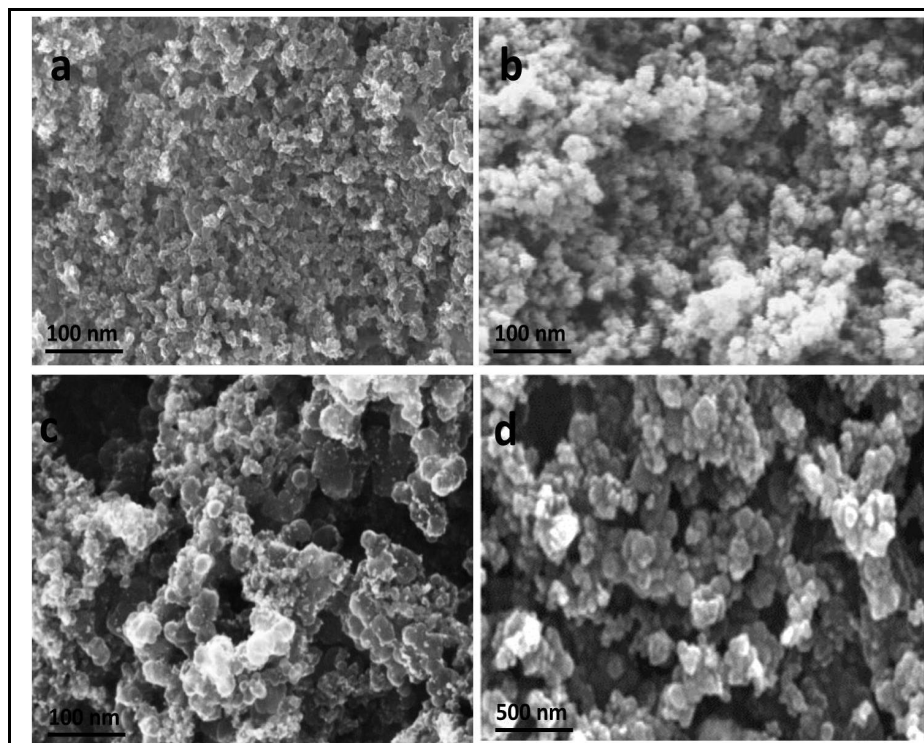


Fig. 3 SEM images of a) Pt/C, b) Pt–Fe/C, c) Pt–Ru/C and d) Pt–Ru–Fe/C catalysts

Transmission electron microscopy (TEM)

The TEM images of the Pt/C, Pt–Fe/C, Pt–Ru/C and Pt–Ru–Fe/C catalysts are presented in Fig. 4a–d, respectively. It indicates that catalysts consist of nano sized metal particles, uniformly dispersed on carbon

support. It can be seen from the images that the metal particle sizes of each sample are less than 5 nm, and they are of spherical shape and slightly agglomerated. Agglomeration might be ascribed to fast reduction process [27]. The average size of the metal particles on the prepared catalysts was evaluated from an ensemble of 200 particles in an arbitrarily chosen area of the corresponding TEM images. In comparison to Pt-Fe/C (50:50) and Pt-Ru-Fe/C (70:10:20) the mean particle size of Pt-Ru-Fe/C (70:15:15) and Pt-Ru-Fe/C (70:20:10) were smaller. The particle size distribution of these catalysts is shown in Table 1 in accordance to the TEM images. The particle size for Pt-Ru-Fe/C (70:10:20) varies from 1 to 14 nm, with a mean diameter of 2.5 nm. In the size range of 2 to 14 nm, the mean particle size for Pt-Ru-Fe/C (70:15:15) and Pt-Ru-Fe/C (70:20:10) is 2.2 nm and 2.0 nm respectively. Similarly, for Pt-Fe/C (50:50) the mean particle size is 3.7 nm and size distribution is from 1 to 14 nm. The mean particle size found by TEM image and XRD analysis were similar. Further, it was observed that the particle size of Pt-Ru/C (50:50) was similar to that of Pt-Fe/C (50:50).

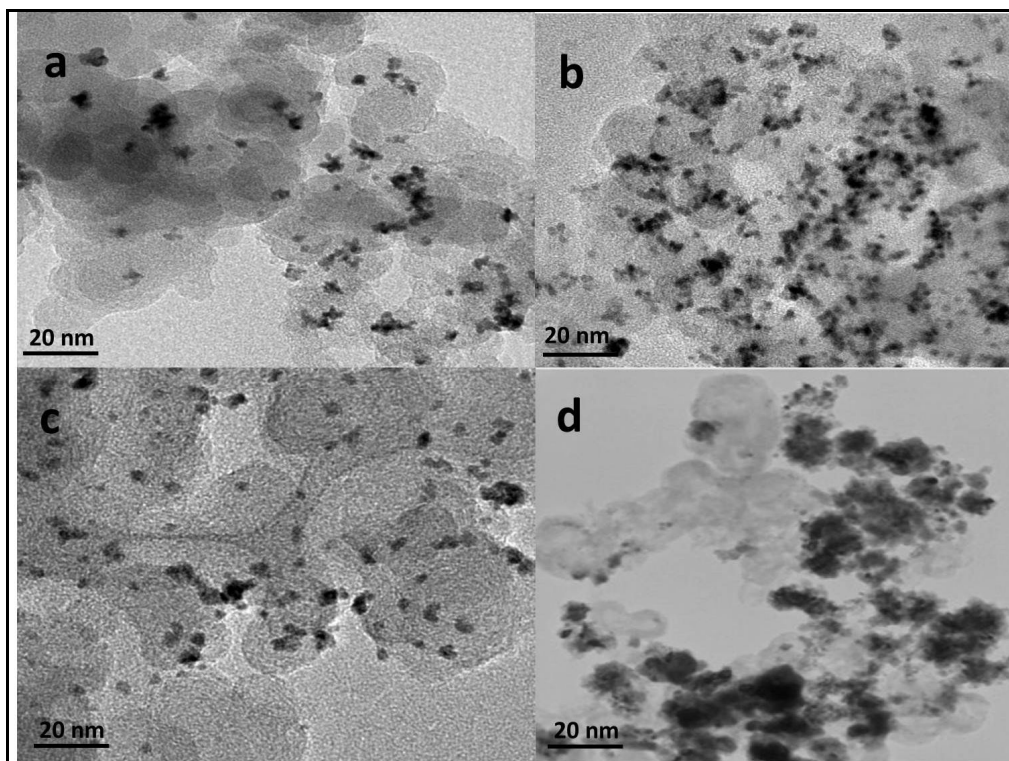


Fig. 4 TEM images of a) Pt/C, b) Pt-Fe/C, c) Pt-Ru/C and d) Pt-Ru-Fe/C catalysts

Energy dispersive X-ray (EDX) analysis

The EDX analyses of all the Pt/C, Pt-Fe/C, Pt-Ru/C, and Pt-Ru-Fe/C catalysts are shown in Fig. 5. The EDX results are shown in Table 1. The catalysts prepared had the desired elements with some variation in composition. The EDX results of the binary Pt-Fe/C and Pt-Ru/C and the ternary Pt-Ru-Fe/C catalysts are very close to the nominal values, which indicate that the metals were loaded onto the carbon support without obvious loss.

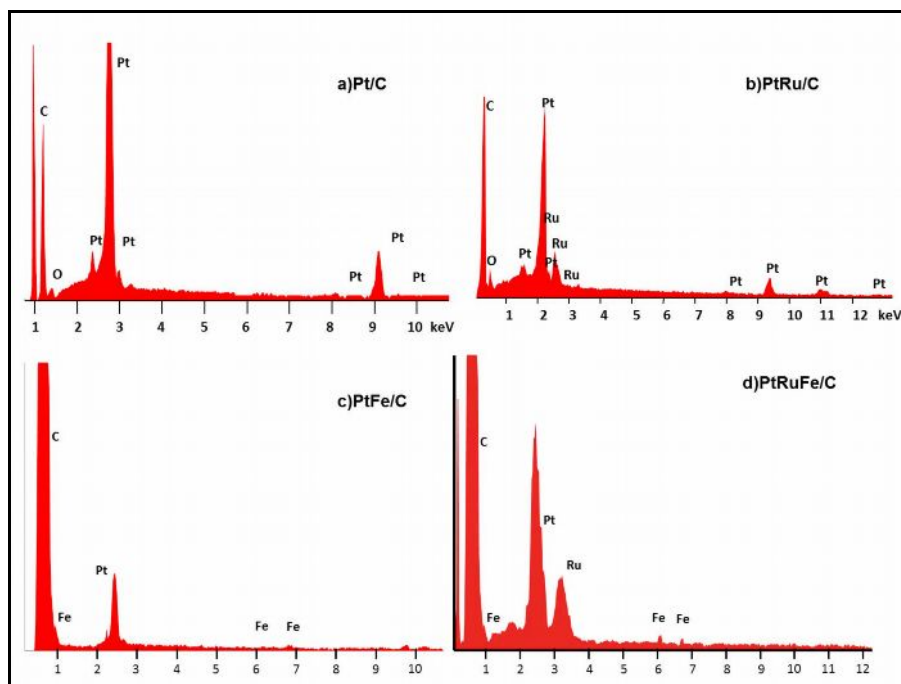


Fig. 5 EDX spectra of a) Pt/C, b) Pt-Fe/C, c) Pt-Ru/C and d) Pt-Ru-Fe/C catalysts

Electrochemical characterization

Cyclic voltammetry (CV)

Fig. 6a shows the cyclic voltammetry of Pt-Fe/C, Pt-Ru/C and Pt-Ru-Fe/C electrocatalysts deposited onto glassy-carbon electrode in the absence of methanol. The voltammograms of the electrocatalysts do not display a well-defined hydrogen adsorption-desorption region (0–0.4 V) as observed for Pt alloys [18]. The current for all the alloys in the double layer region (0.4–0.8 V vs. Ag/AgCl) is larger compared to pure Pt. The voltammograms behavior is characteristic of binary and ternary electrocatalysts containing transition metals [28]. The current values were normalized per gram of platinum, considering that methanol adsorption and dehydrogenation occur only on platinum sites at room temperature [29].

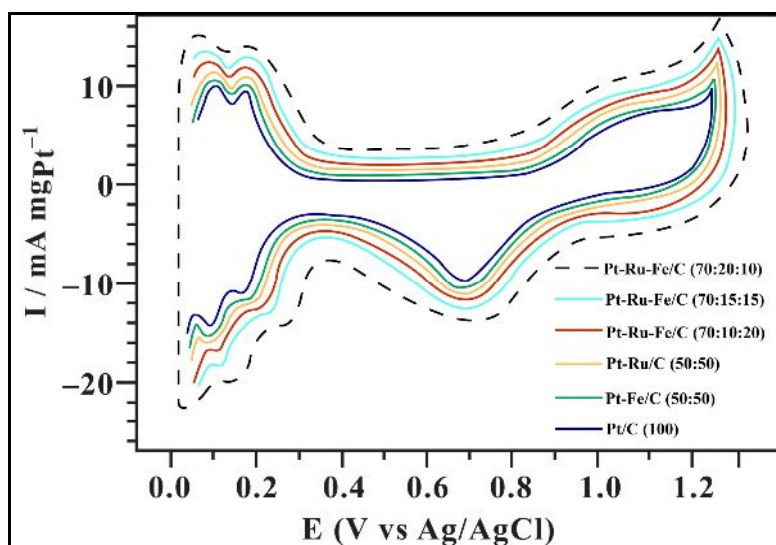


Fig. 6a Cyclic voltammetry of Pt/C (100), Pt-Fe/C (50:50), Pt-Ru/C (50:50), Pt-Ru-Fe/C (70:10:20), Pt-Ru-Fe/C (70:15:15) and Pt-Ru-Fe/C (70:20:10) electrocatalysts in 0.5 M H₂SO₄ at room temperature with a scan rate of 50 mV/s

In order to investigate the electrocatalytic activity of the catalysts for methanol oxidation, the electrochemically active surface area (S_{EAS}) was estimated using different procedures; namely CO adsorption ($S_{EAS/CO}$), hydrogen adsorption/desorption charge ($S_{EAS/H}$), and roughness of electrodes. The S_{EAS} values of the electrocatalysts were calculated by using Eq. (4) and Eq. (5) [20,30-31].

$$S_{EAS/H}(m^2/g) = \frac{Q_H(\mu C/cm^2)}{210(\mu C/cm^2) \times 0.77 \times [Pt]} \quad (4)$$

$$S_{EAS/CO}(m^2/g) = \frac{Q_{CO}(\mu C/cm^2)}{420(\mu C/cm^2) \times [Pt]} \quad (5)$$

Where Q_H and Q_{CO} are the charges corresponding to desorption of hydrogen and CO on the Pt surface respectively, $[Pt]$ (mg/cm^2) is the Pt loading on the electrode surface, $210 \mu C/real\ cm^2$ and $420 \mu C/real\ cm^2$ is the charge required to oxidize a monolayer of hydrogen and CO respectively on the Pt surface, 0.77 is the hydrogen monolayer coverage [32]. The roughness of each electrode is calculated by dividing S_{EAS} obtained with the apparent surface area. Estimation of the electrode roughness and S_{EAS} values are shown in Table 2. Based on these values, the highest electrochemically active area is achieved for the ternary electrocatalysts.

Table 2 Comparison of hydrogen desorption charge and carbon monoxide desorption charge, and its electrochemical active surface area (S_{EAS}) and electrode roughness.

Catalyst	$Q_H/\mu C$	$Q_{CO}/\mu C$	Electrode real surface area (cm^2)	$S_{EAS/H}$ (m^2gPt^{-1}) ^a	$S_{EAS/CO}$ (m^2gPt^{-1}) ^a	Roughness
Pt/C (100)	404	1176	2.8	25	28	78.4
Pt-Fe/C (50:50)	243	735	1.7	30	35	47.6
Pt-Ru/C (50:50)	251	777	1.8	31	37	50.4
Pt-Ru-Fe/C (70:10:20)	464	1352	3.2	41	46	89.6
Pt-Ru-Fe/C (70:15:15)	498	1411	3.4	44	48	95.2
Pt-Ru-Fe/C (70:20:10)	521	1441	3.4	46	49	95.2

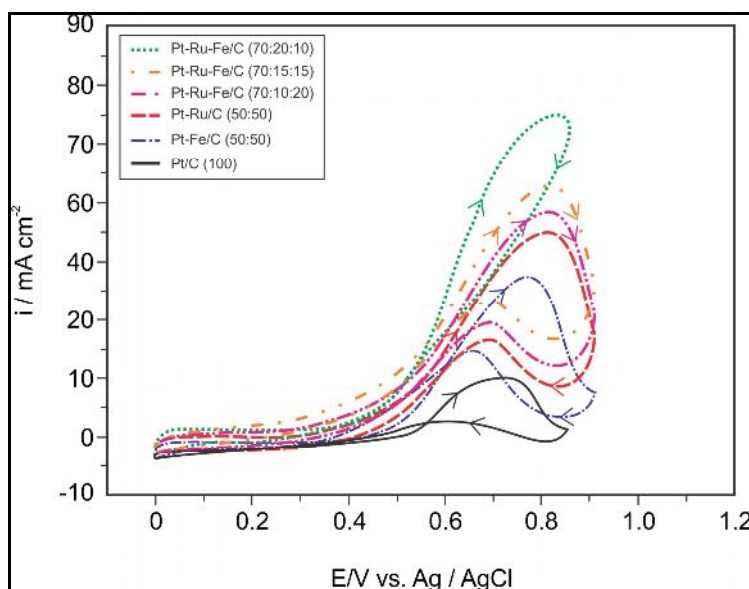
^aThe electrochemical active surface area ($S_{EAS/H}$ and $S_{EAS/CO}$) were calculated from Eq. (4) and Eq. (5).

Fig. 6b shows the cyclic voltammograms (CV) of methanol oxidation under acidic conditions (1.0 M C_2H_5OH and 0.5 M H_2SO_4) catalyzed by Pt-Fe/C (50:50), Pt-Ru/C (50:50), Pt-Ru-Fe/C (70:10:20), Pt-Ru-Fe/C (70:15:15) and Pt-Ru-Fe/C (70:20:10) catalysts. There were three oxidation peaks when methanol CV was carried out on the Pt/C catalyst (vs. Ag/AgCl), two during the forward scan and one during the reverse scan. The peak in the forward scan is associated with the methanol oxidation, and the peak in the reverse scan is related to the oxidation of carbonaceous intermediate products from incomplete methanol oxidation. Table 3 summarizes the CV results of the prepared electrocatalysts including the positive peak potentials and the corresponding peak current densities of EOR.

Table 3 CV results of Pt/C, Pt–Ru/C, Pt–Fe/C and Pt–Ru–Fe/C electrocatalysts at room temperature

Catalyst	Scan rate 50 mV/s	
	Positive peak potential (V vs. Ag/AgCl)	Peak current density (mA/cm ²)
Pt/C (100)	0.795	8.497
Pt–Fe/C (50:50)	0.835	13.107
Pt–Ru/C (50:50)	0.820	12.412
Pt–Ru–Fe/C (70:20:10)	0.785	17.796
Pt–Ru–Fe/C (70:15:15)	0.750	23.603
Pt–Ru–Fe/C (70:20:10)	0.760	34.499

The CV results show that pure Pt₁₀₀/C catalysts (Fig. 6b) do not behave as an appropriate anode for EOR due to its poisoning by strongly adsorbed intermediates such as CO [33]. However, the introduction of Ru and Fe promotes the electrocatalytic activity. The EOR starts at approximately 0.3 V on the Pt–Fe/C (50:50) electrode, while the onset potential on Pt–Ru/C (50:50) was noted at 0.35 V vs. Ag/AgCl. This observation can be explained by the more pronounced oxophilic character of iron at low potentials in comparison with ruthenium [16]. Furthermore, the presence of both co-catalysts, Fe and Ru, significantly reduced the onset potential to approximately 0.2 V vs. Ag/AgCl (i.e. shifted to negative potential by 0.2 V in comparison to Pt/C (0.4 V vs. Ag/AgCl) and raised the current density at the Pt–Ru–Fe/C electrocatalysts. The superior activity of the ternary Pt–Ru–Fe/C electrocatalysts can be attributed to the modification of electronic properties of platinum and to the presence of iron oxide species resulting in a combination of electronic effect and bifunctional mechanism [34-36]. Again, the ternary compositions (Pt–Ru–Fe/C (70:20:10)) presented much higher current densities than the other catalysts, indicating that the best performance was achieved with lower Fe atomic ratios, which confirmed the previous results showing that low Fe atomic ratios (close to 10%) in Pt–Fe electrocatalysts lead to higher activities towards methanol oxidation [37-38]. On the other hand, addition of Ru to Pt (Pt–Ru/C) had a little effect, whereas addition of Ru to Pt–Fe greatly enhanced the electrocatalytic activity.

**Fig. 6b Cyclic voltammetry of Pt/C, Pt–Ru/C, Pt–Fe/C and Pt–Ru–Fe/C electrocatalysts in 1.0 M methanol and 0.5 M H₂SO₄ at room temperature with a scan rate of 50 mV/s**

Chronoamperometry (CA)

The Pt–Fe/C, Pt–Ru/C, and Pt–Ru–Fe/C electrocatalyst performances for methanol oxidation were studied by chronoamperometry at 0.4V for 30 minutes, to evaluate both the electrocatalytic activity of the catalysts and the poisoning of the active surface under continuous operation conditions. Fig. 7 shows

representative chronoamperograms obtained for the different electrocatalysts whose current densities were normalized by Pt mass. During the first few minutes, there was a sharp decrease in the current density and after some time, it becomes relatively stable. This behavior can be explained assuming that initially the active sites are free from adsorbed methanol molecules, but a new adsorption of methanol molecules is a function of the liberation of the active sites by methanol oxidation and intermediate species (CO, CH_x, CH₃CHO and CH₃COOH) formed during the first minutes, which are responsible for poisoning of the catalytic sites [35].

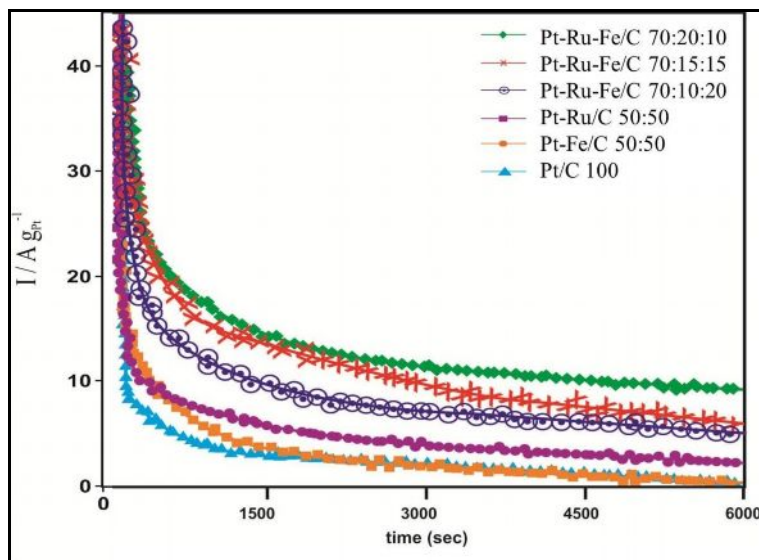


Fig. 7 Current vs. time plots for the electro-oxidation of 1.0 M methanol in 0.5 M H₂SO₄ at 0.4 V vs. Ag/AgCl on various Pt-based/C catalysts

The ternary Pt–Ru–Fe/C (70:10:20), Pt–Ru–Fe/C (70:15:15) and Pt–Ru–Fe/C (70:20:10) electrocatalysts gave higher current than the binary Pt–Fe/C (50:50) and Pt–Ru/C (50:50) electro-catalysts. Higher current obtained for the ternary electrocatalysts may be explained by the operation of a beneficial synergistic effect between Fe and Ru. This may indicate an increase in structural defects or roughness, making the ternary electrocatalysts better candidates for methanol electro-oxidation. Furthermore, the addition of Ru to the Pt–Fe alloy electrocatalysts can lead to an increase in the surface oxophilic character, thus increasing the Fe–O bond strength and the acidity of the Fe–OH sites, which can favor methanol electro oxidation at lower potentials [39]. On the other hand, Ru atoms may disturb the Pt–Fe sites and orbital symmetries, thus affecting the orbital spatial distribution and the methanol electro-oxidation rate [40]. Cunha *et al.* [35] pointed out the presence of the oxophilic metals such as Ru and Fe in the composition of the Pt-based electrocatalysts enhances methanol oxidation. Similar results were observed by Neto *et al.* [12] and Jiang *et al.* [41] for alcohol oxidation by using catalysts prepared by alcohol-reduction process. These observations suggest that the performance of Pt–Ru–Fe/C electrocatalysts depends greatly on its atomic ratios and its preparation procedure.

Single cell performance

The Pt–Fe/C (50:50), Pt–Ru/C (50:50), Pt–Ru–Fe/C (70:10:20), Pt–Ru–Fe/C (70:15:15), Pt–Ru–Fe/C (70:20:10) and Pt/C (100) catalysts were evaluated as anode catalysts for methanol electro-oxidation by single membraneless methanol fuel cell (MLMFC), and the data are presented in Fig. 8. When Pt/C (100) was used as the anode catalyst, the performance of single cell was poor. The open-circuit potential (OCP) was 0.54 V, far less than the reversible OCP (1.145 V) [34], which was mainly attributed to poor catalytic activity towards methanol electro-oxidation. The maximum output power density for Pt/C (100) is 4.42 mW/cm². The results of MLMFC adopting to different catalysts are summarized in Table 4. When the current was normalized to the geometric area of single cell, it was observed that the cell performance of Pt–Ru–Fe/C (70:20:10) catalyst was better than other catalysts. In the low current discharging region, the power drawn from single cell was almost the same for all catalysts except Pt–Ru/C (50:50) and Pt/C (100). However, as the voltage reach around 0.3 V Pt–Ru–Fe/C (70:20:10) started drawing more current in comparison to others. In addition, there was a rapid initial fall in cell voltage for all catalysts, which was due to the slow initial methanol electro-oxidation reaction at the electrode surface. After an initial drop of 50 mV the change in slope of the polarization curve for

Pt–Ru–Fe/C (70:20:10) decreased, and it started drawing more current. This event can be attributed to the more effective catalytic ability of Pt–Ru–Fe/C (70:20:10), once the EOR reaction is initiated. Based on the peak power density drawn from a single cell, Pt–Ru–Fe/C (70:20:10) is the best anode catalyst with a peak power density value of 34.97 mW/cm².

Table 4 Summary of performance of single fuel cell tests using (2 mg cm⁻² catalyst loading, 40 wt% catalyst on carbon)

Anode Catalysts	Open circuit Potential (V)	Maximum power density (mW/cm ²)	Maximum Current density (mA/cm ²)
Pt/C (100)	0.54	4.42	43.90
Pt–Fe/C (50:50)	0.58	12.48	100.29
Pt–Ru/C (50:50)	0.6	17.11	115.85
Pt–Ru–Fe/C (70:20:10)	0.63	24.22	166.09
Pt–Ru–Fe/C (70:15:15)	0.66	30.11	194.63
Pt–Ru–Fe/C (70:20:10)	0.73	34.97	213.55

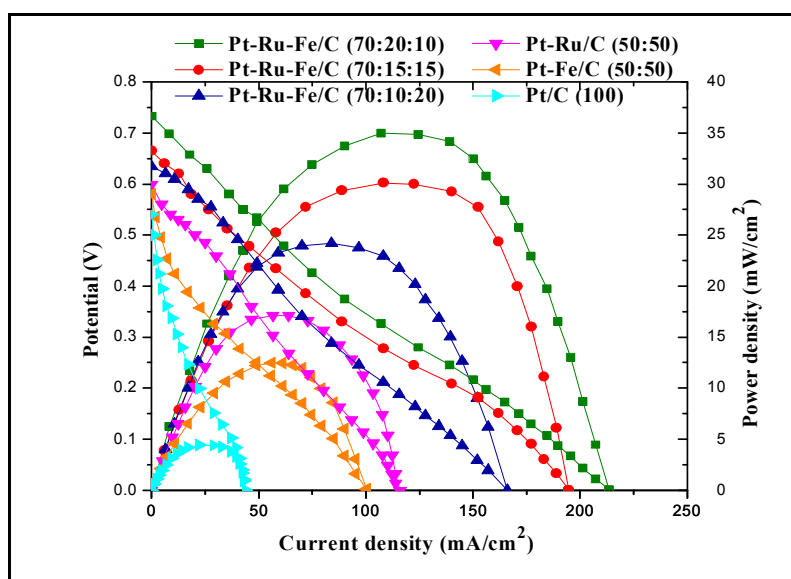


Fig. 8 Cell voltage–current density characteristics and power density of MLMFC using the Pt-based binary and ternary anodes (2 mg cm⁻² catalyst loading, 40 wt.% catalyst on carbon)

Pt–Fe/C (50:50) (Fe 50 at.%), Pt–Ru–Fe/C (70:15:15) (Fe 15 at.%), Pt–Ru–Fe/C (70:10:20) (Fe 10 at.%) and Pt–Ru–Fe/C (70:20:10) (Fe 20 at.%) showed OCV of 0.58 V, 0.63 V, 0.66 V and 0.73 V respectively in comparison to Pt–Ru/C (50:50) and Pt/C (100) which showed OCV of 0.6 V and 0.54 V, respectively. The comparison of both the bimetallic catalysts showed that peak power density of Pt–Ru/C (50:50) (17.11 mW/cm²) was higher than the Pt–Fe/C (50:50) (12.48 mW/cm²).

The addition of Ru is conducive to breaking of C–C bonds in Pt–Ru–Fe/C (70:10:20), but the lesser percentage of Ru and higher percentage of Fe in Pt–Ru–Fe/C (70:15:15) and Pt–Ru–Fe/C (70:20:10) blocks the further oxidation of intermediates. This may be due to adsorption of the intermediates on the active sites of the catalysts. In the ternary combinations of Pt, Fe, and Ru, the addition of Fe increases the cell performances. It is seen that for Pt–Ru/C (50:50) and Pt–Ru–Fe/C combination containing 10, 15, and 20 atomic ratios of Ru, the peak power densities are 17, 11, 24.22, 30.11 and 34.97 mW/cm², respectively. This indicates that only a small amount of Fe in Pt–Ru–Fe/C catalyst helps in electro-oxidation of methanol.

Conclusions

In this work, we observed that the co-impregnation reduction method could be effectively used for the preparation of Pt–Fe/C, Pt–Ru/C and Pt–Ru–Fe/C electrocatalysts for methanol oxidation. The X-ray diffractograms of the Pt–Ru/C electrocatalyst showed a typical fcc structure of the Pt alloys. The Pt–Fe/C and Pt–Ru–Fe/C electrocatalysts showed a typical fcc structure of platinum alloys in the presence of a separated FeO₂ phase. The Pt metal was the predominant material in all the samples, with peaks attributed to the face-centered cubic (fcc) crystalline structure. The SEM and TEM analysis indicated that the catalysts on Vulcan XC-72 carbon support are uniformly dispersed having size of 2 – 5 nm. Additionally, the SEM images confirm the porous structure of the catalysts prepared. EDX analysis indicated that the experimental composition is in agreement with the nominal composition of the catalyst, which confirm the formation Pt–Ru–Fe/C, Pt–Ru/C and Pt–Fe/C metal catalysts having typical Pt crystalline structure and the formation of Pt–Fe alloy. Cyclic voltammetry results showed that Pt–Ru–Fe/C (70:10:20) is more active in methanol electro-oxidation than other catalysts. The onset potential for this reaction was found to be 0.2 V vs. Ag/AgCl, which suggests that activation takes place at the electrode surface by a ligand effect. Chronoamperometry results showed that the ternary Pt–Ru–Fe/C (70:10:20), Pt–Ru–Fe/C (70:15:15) and Pt–Ru–Fe/C (70:20:10) catalysts gave higher current than the binary Pt–Ru/C (50:50) and Pt–Fe/C (50:50) catalysts at steady condition. The enhanced methanol oxidation activity by the ternary Pt–Ru–Fe catalyst was mainly ascribed to the synergistic effect between Fe and Ru, and to the smaller particle size. In this work, for the first-time carbon-supported binary Pt–Fe/C, Pt–Ru/C and ternary Pt–Ru–Fe/C anode catalysts were successfully tested in a single membraneless fuel cell using 1.0 M methanol as the fuel and 0.1 M sodium percarbonate as the oxidant in the presence of 0.5 M H₂SO₄ as the electrolyte. Based on peak power density drawn from a single cell, Pt–Ru–Fe/C (70:20:10) is the best anode catalyst with peak power density value of 34.97 mW/cm² among the catalysts tested. Further work is necessary to characterize the catalysts using different surface analysis techniques and to conduct tests of these electrocatalysts in microfluidic membraneless fuel cells.

References

1. Choban ER, Markoski LJ, Wieckowski A and Kenis PJA. Microfluidic fuel cell based on laminar flow. *J. Power Sources* 2004; 128:54-60.
2. Narayanan SR and Valdez TI. Handbook of fuel cells— Fundamentals, technology and application, edited by W. Vielstich, A. Lamm, and H. A. Gasteiger ~Wiley, Hoboken, NJ, 2003;4: p.1133.
3. Kjeang E, Djilali N and Sinton D. Microfluidics fuel cells: A review. *Journal of Power Sources* 2009;186:353-369.
4. Ferrigno R, Stroock AD, Clark TD, Mayer M, and Whitesides GM. Membraneless vanadium redox fuel cell using laminar flow. *J. Am. Chem. Soc.* 2002;124:12930-12931.
5. Lamy C, Belgsir EM, Le ger J-M. Electrocatalytic oxidation of aliphatic alcohols: application to the direct alcohol fuel cell (DAFC). *J Appl Electrochem* 2001;31:799-801.
6. Wang F, Zheng Y and Guo Y. The promoting effect of europium on PtSn/C catalyst for ethanol oxidation. *FUEL CELLS* 2010;6:1100–1107.
7. Zhou WJ, Zhou B, Li WZ, Zhou ZH, Song SQ and Sun GQ. Performance comparison of low-temperature direct alcohol fuel cells with different anode catalysts. *J Power Sources* 2004;126:16-22.
8. Colmati F, Antolini E and Gonzalez ER. Ethanol oxidation on a carbon-supported Pt₇₅Sn₂₅ electrocatalyst prepared by reduction with formic acid: Effect of thermal treatment. *Appl Catal B* 2007;73:106-115.
9. Zhou WJ, Li WZ, Song SQ, Zhou ZH, Jiang LH and Sun GQ. Bi- and tri-metallic Pt-based anode catalysts for direct ethanol fuel cells. *J Power Sources* 2004;131:217-23.
10. Delbecq F and Vigne F. Acetaldehyde on Pt (111) and Pt/Sn (111): a DFT study of the adsorption structures and of the vibrational spectra. *J Phys Chem B* 2005;109:10797-10806.
11. Tayal J, Rawat B and Basu S. Effect of addition of rhenium to Pt-based anode catalysts in electro-oxidation of ethanol in direct ethanol PEM fuel cell. *International Journal of Hydrogen energy* 2012;37:4597-4605.
12. Neto AO, Dias RR, Tusi MM, Linardi M and Spinace EV. Electro-oxidation of methanol and ethanol using PtRu/C, PtSn/C and PtSnRu/C electrocatalysts prepared by an alcohol-reduction process. *Journal of power sources* 2007;166:87–91.

13. Jeon MK, Lee KR, Daimon H, Nakahara A and Woo SI. Pt₄₅Ru₄₅M₁₀/C (M = Fe, Co, and Ni) catalysts for methanol electro-oxidation. *Catalysis Today* 2008;132:123–126.
14. Chen W, Wei X and Zhang Y. A comparative study of tungsten-modified PtRu electrocatalysts for methanol oxidation. *International journal of hydrogen energy* 2014;39:6995–7003.
15. Scofield ME, Koenigsmann C, Wang L, Liua H and Wong SS. Tailoring the composition of ultrathin, ternary alloy PtRuFe nanowires for the methanol oxidation reaction and formic acid oxidation reaction, *Energy Environ. Sci.* 2015;8:350 – 363.
16. Yang B, Lu Q, Wang Y, Zhuang L, Lu J and Liu P. Simple and low-cost preparation method for highly dispersed PtRu/C catalysts. *Chem Mater* 2003;15:3552-3557.
17. Spinace EV, Linardi M and Neto AO. Co-catalytic effect of nickel in the electro-oxidation of ethanol on binary Pt–Sn electrocatalysts. *Electrochemistry Communications* 2005;7:365–369.
18. Radmilovic V, Gasteiger HA and Ross Jr. PN. Structure and chemical composition of a supported Pt–Ru electrocatalyst for methanol oxidation. *J. Catal.* 1995;154:98–106.
19. Beyhan S, Leger J-M and Kadırgan F. Pronounced synergetic effect of the nano-sized PtSnNi/C catalyst for ethanol oxidation in direct ethanol fuel cell *Applied Catalysis B: Environmental* 2013;130:305–313.
20. Arun A, Gowdhamamoorthi M, Ponmani K, Kiruthika S and Muthukumar B. Electrochemical characterization of Pt-Ru-Ni/C anode electrocatalyst for methanol electrooxidation in membraneless fuel cells. *RSC Advances* 2015;5:49643-49650.
21. Gowdhamamoorthi M, Arun A, Kiruthika S and Muthukumar B. Perborate as novel fuel for enhanced performance of membraneless fuel cells. *Ionics* 2014;20:1723-1728.
22. Arun A, Gowdhamamoorthi M, Kiruthika S and Muthukumar B. Analysis of membraneless methanol fuel cell using percarbonate as an oxidant, *J of The Electrochemical Society* 2013;161:F1-F7.
23. Ponmani K, Durga S, Gowdhamamoorthi M, Kiruthika S and Muthukumar B. “Influence of fuel and media on membraneless sodium percarbonate fuel cell”, *Ionics*, 2014;20:1579-1589.
24. Cotton FA and Wilkinson G. *Advanced inorganic chemistry*. Wiley Interscience, New York, 1988;p 812.
25. Jayashree RS, Yoon SK, Brushett FR, Lopez-Montesinos PO, Natarajan D, Markoski LJ and Kenis PJA. On the performance of membraneless laminar flow-based fuel cells, *Journal of Power Sources* 2010;195:3569–3578.
26. Spinace EV, Neto AO, Vasconcelos TRR and Linardi M. Electro-oxidation of ethanol using PtRu/C electrocatalysts prepared by alcohol-reduction process. *J. Power Sources* 2004;137:17-23.
27. Zhou WJ, Song SQ, Li WZ, Zhou ZH, Sun GQ and Zin Q. Direct ethanol fuel cells based on PtSn anodes: the effect of Sn content on the fuel cell performance. *J Power Sources* 2005;140:50-58.
28. Ribeiro J, dos Anjos DM, Kokoh KB, Coutanceau C, Leger J-M, Olivi P, de Andrade AR and Tremiliosi-Filho G. Carbon-supported ternary PtSnIr catalysts for direct ethanol fuel cell. *Electrochimica Acta* 2007;52:6997–7006.
29. Zhou Z, Wang S, Zhou W, Wang G, Jiang L, Li W, Shuquin S, Liu J, Sun G and Xin Q. Novel synthesis of highly active Pt/C cathode electrocatalyst for direct methanol fuel cell. *Chem Commu* 2003;2003:394-395.
30. Bonesi A, Moreno MS, Triaca WE and Castro Luna AM. Modified catalytic materials for ethanol oxidation. *International Journal of Hydrogen Energy* 2010;35:5999-6004.
31. Ribadeneira E and Hayos BA. Evaluation of Pt-Ru-Ni and Pt-Sn-Ni catalysts as anodes in direct ethanol fuel cells. *Journal of Power Sources* 2008;180:238-242.
32. Biegler T, Rand DAJ and Woods R. Limiting oxygen coverage on platinumized platinum; Relevance to determination of real platinum area by hydrogen adsorption. *Journal of Electroanalytical Chemistry* 1971;29:269-277.
33. Vigier F, Coutanceau C, Hahn F, Belgsir EM and Lamy C. On the mechanism of ethanol electro-oxidation on Pt and PtSn catalysts: electrochemical and in situ IR reflectance spectroscopy studies. *J Electroanal Chem* 2004;563:81-89.
34. Antolini E, Colmati F and Gonzalez ER. Effect of Ru addition on the structural characteristics and the electrochemical activity for ethanol oxidation of carbon supported Pt–Sn alloy catalysts. *Electrochem. Commun.* 2007;9:398–404.
35. Cunha EM, Ribeiro J, Kokoh KB and de Andrade AR. Preparation, characterization and application of Pt-Ru-Sn/C trimetallic electrocatalysts for ethanol oxidation in direct fuel cell, *International journal of hydrogen energy* 2011;36:11034-11042.

36. Rousseau S, Coutanceau C, Lamy C and Leger J-M. Direct ethanol fuel cell (DEFC): Electrical performances and reaction products distribution under operating conditions with different platinum-based anodes. *J. Power Sources* 2006;158:18-24.
37. Lamy C, Rousseau S, Belgsir E, Coutanceau C and Leger J-M. Recent progress in the direct ethanol fuel cell: development of new platinum–tin electrocatalysts. *Electrochim Acta* 2004;49:3901–3908.
38. Vigier F, Coutanceau C, Perrard A, Belgsir E and Lamy C. Development of anode catalysts for a direct ethanol fuel cell. *J. Appl. Electrochem.* 2004;34:439–446.
39. Chen G, Delafuente DA, Sarangapani S and Mallouk TE. Combinatorial discovery of bifunctional oxygen reduction-water oxidation electrocatalysts for regenerative fuel cells. *Catal Today* 2001;67:341-55.
40. Woodward RB and Hoffman R. Selection rules for concerted cycloaddition reactions. *J American Chem Soc.* 1965;87:2046-2048.
41. Jiang L, Sun G, Sun S, Liu J, Tang S, Li H, Zhou B and Xin Q. Structure and chemical composition of supported Pt-Sn electrocatalysts for ethanol oxidation. *Electrochim Acta* 2005;50:5384-5389.
